Available online at www.sciencedirect.com

ScienceDirect

Procedia CIRP 119 (2023) 752–757

www.elsevier.com/locate/procedia

33rd CIRP Design Conference

Method for the design of additively manufactured inner channels intended for adhesive application

M. Ascher [a,*], G.A. Pang[a], R. Späth[a]

[a] Universität der Bundeswehr München, Werner-Heisenberg-Weg 39, 85577 Neubiberg, Germany

* Corresponding author. Tel.: +49-89-6004-3296. E-mail address: michael.ascher@unibw.de

Abstract

Joining of metal parts manufactured by laser beam powder bed fusion (PBF-LB/M) eliminates the inherent size restriction of this additive manufacturing process and reduces the manufacturing effort. Adhesive bonding presents great potential for joining of PBF-LB/M parts, as there are no constraints on the shape of the connecting surfaces, as long as the adhesive can be applied. The freedom of design underlying the PBF-LB/M process enables the construction of inner channels in the parts, which can facilitate the adhesive application. The adhesive can be injected into a single inlet on the exterior of a part and directed through inner channels before leaking from multiple outlets into the adhesive fill gap between the pre-aligned adherents. To avoid insufficient adhesive distribution and air inclusions in the adhesive fill gap, both of which reduce the bond strength, a methodical approach for the design of inner channels intended for adhesive application by injection is required. This work provides a corresponding design method based on the theory of fluid mechanics. Moreover, an example case of a PBF-LB/M sleeve to be joined to a circular tube is presented. Results from a CFD analysis show that the inner channels designed using the presented method lead to excellent coverage of the adhesive fill gap with adhesive and minimal air inclusions.

Keywords: additive manufacturing; powder bed fusion; adhesive bonding; inner channel; injection bonding

1. Introduction

In laser beam powder bed fusion of metal (PBF-LB/M), the limited build space of the manufacturing equipment restricts the maximum size of a single PBF-LB/M part [1]. Further restrictions include the need for support structures to reduce thermal stress induced distortion [2], and requirements regarding the removal of powder residues [3]. Both are limiting the achievable geometrical complexity of PBF-LB/M parts and increasing manufacturing cost due to additional post-processing efforts [4]. Joining of multiple PBF-LB/M parts can be an effective way of repealing size limitations, increasing the freedom of design, and decreasing manufacturing cost [5]. Moreover, in many applications, the benefits of the PBF-LB/M process are only needed in certain areas of a structure. Therefore, non-PBF-LB/M parts (e.g., fiber reinforced plastic parts) can contribute to achieving the desired characteristics of the structure by being joined with PBF-LB/M parts.

Adhesive bonding is ideal for many joining applications due to the low adhesive weight and lack of restrictions on both the connecting surface´s geometry and the material of the adherends. The adhesive application process has a large influence on the strength and reliability of the joint, but the correct implementation often poses a major technical challenge [6]. The conventional process of pre-applying the adhesive to the connecting surfaces is highly error prone, as it carries the risk of partially pushing out adhesive while merging and aligning the adherents. This is likely to result in application errors such as underdosing or insufficient distribution, and therefore, reduced and unpredictable bond strength.

A unique design feature in additive manufacturing (AM) is the ability to manufacture complex inner channel geometries

2212-8271
10.1016/j.procir.2023.02.164

(e.g., conformal cooling channels [3,7]) that can deliver injected adhesive into the fill gap between the aligned adherents [8]. As the PBF-LB/M process involves the occurrence of sagging and dross [9], the minimum manufacturable radius of horizontally extending inner channels is limited due to the material and machine used [10]. A 45°-droplet-like shape for the cross section of the inner channels is, therefore, recommended [10–12]. Multiple outlets from the inner channels into the adhesive fill gap are typically needed to ensure complete coverage with adhesive [13]. These can be connected to a single accessible adhesive inlet. The specific number and position of adhesive outlets to the fill gap depends on multiple factors and determines the layout of the inner channels in the PBF-LB/M part.

In this work, a method based on the theory of fluid mechanics to design inner channels for adhesive application by injection is presented. This method was applied to a circular adhesive single lap joint (SLJ) between a PBF-LB/M sleeve of aluminum alloy AlSi10Mg (outer adherent) and a circular carbon fiber reinforced plastic (CFRP) tube (inner adherent) with a 2-component construction adhesive based on epoxy resin (3M Scotch-Weld DP490).

2. Design method

The adhesive fill gap is defined as the volume between the pre-aligned adherends that needs to be filled with adhesive to create a joint. The adhesive is to be applied by injection into an accessible adhesive inlet, which is not located directly at the adhesive fill gap. By means of inner channels, the adhesive is introduced into the adhesive fill gap through multiple adhesive outlets. The objective of the method is to design the inner channels in four sequential phases to ensure complete coverage of the adhesive fill gap with adhesive. Figure 1 shows a flow chart of the method and a general schematic of an arbitrary joint.

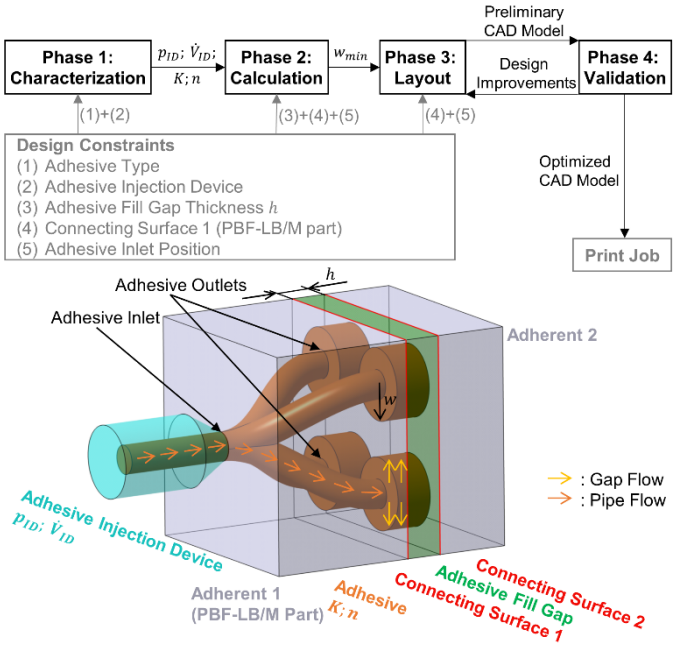

Figure 1: Method for the design of inner channels for adhesive application (top) and schematic of an arbitrary joint (bottom)

Prior to beginning the design method, the intended adhesive and injection device must be identified, along with the position of the intended adhesive inlet, form of the connecting surface of the PBF-LB/M part and thickness of the adhesive fill gap h (see Figure 1). These provide the constraints for the design method. In Phase 1, the maximum pressure p_{ID} and maximum volumetric flow rate $\dot{V}_{ID}$ of the injection device are determined, as well as the flow consistency index K and the flow behavior index n, which describe the viscosity characteristics of the adhesive. In Phase 2, the adhesive´s minimum propagation radius w_{min} into the adhesive fill gap is calculated based on the pressure loss resulting from the adhesive flow. Phase 3 specifies how to position a suitable number of adhesive outlets to the adhesive fill gap to ensure complete coverage of the fill gap. Connecting the adhesive outlets to the adhesive inlet through inner channels in the PBF-LB/M part results in a CAD model of the PBF-LB/M part, which includes a preliminary inner channel layout. The preliminary inner channel layout´s ability to completely cover the adhesive fill gap with adhesive is verified with a computational fluid dynamics (CFD) simulation or physical visualization models, which is described in Phase 4. As part of an iterative optimization process, design improvements resulting from Phase 4 can be used to optimize Phase 3. All the phases are described in general terms below. In Section 3, they are applied to an example joint.

2.1. Phase 1: Characterization of adhesive and injection device

The adhesive flow in the inner channels and the fill gap is governed by its viscous behavior, which can be represented graphically as a flow curve (shear stress τ as a function of shear rate $\dot{\gamma}$). The Ostwald-de Waele power law [14] describes the viscous behavior of arbitrary fluids according to equation (1), where K is the flow consistency index and n is the flow behavior index.

$$\tau = K|\dot{\gamma}|^n \mathrm{sign}(\dot{\gamma}) \quad (1)$$

The parameters K and n of the adhesive can be determined from a fit to the adhesive´s flow curve by a regression analysis using the method of ordinary least squares [15].

The performance of the injection device is characterized by the maximum pressure p_{ID} and the maximum volumetric flow rate $\dot{V}_{ID}$ that can be produced. The maximum pressure p_{ID} and maximum volumetric flow rate $\dot{V}_{ID}$ of the injection device, along with the adhesive´s flow consistency index K and flow behavior index n are required inputs for the calculation of the adhesive´s radius of propagation in Phase 2. If these values are not provided by the manufacturer, then experimental determination of these characteristics is required.

2.2. Phase 2: Calculation of the adhesive´s minimum radius of propagation in the adhesive fill gap

As the adhesive fill gap thickness h is significantly smaller than the two corresponding transverse dimensions that form the adhesive fill gap, the adhesive spreads concentrically from the adhesive outlets into the fill gap upon exit from the inner

channels (see Figure 1). The adhesive´s radius of propagation in the fill gap is limited by the pressure loss induced by the adhesive flow within the inner channel (pipe flow) and the adhesive fill gap (gap flow). Therefore, the radius of propagation is a function of the maximum pressure p_{ID} and volumetric flow rate $\dot{V}_{ID}$ of the injection device, the flow consistency index K and flow behavior index n of the adhesive, the distance between the adhesive inlet and the fill gap l, the inner channel radius R, and the adhesive fill gap thickness h.

For a fully developed incompressible laminar power law fluid flow through a cylindrical pipe with inner radius R, the velocity profile $u_P(r)$ is described by equation (2), where x and r denote the longitudinal and radial coordinate of the pipe, respectively, and the pressure gradient in the flow direction is given by $|dp/dx|$.

$$u_P(r) = \left(\frac{1}{2K}\left|\frac{dp}{dx}\right|\right)^{1/n}\left(\frac{n}{n+1}\right)\left(R^{\frac{1+n}{n}} - r^{\frac{1+n}{n}}\right) \quad (2)$$

This velocity profile describes the adhesive flow inside the inner channel. The same principle can be used to derive the velocity profile $u_G(y)$ of a concentrically propagating power law fluid between two parallel plates separated by a gap with constant thickness h. The coordinate along the gap thickness is denoted with the variable y and the radial coordinate with the variable ϑ. Equation (3) describes the adhesive flow inside the fill gap.

$$u_G(y) = \left(\frac{1}{2K}\left|\frac{dp}{d\vartheta}\right|\right)^{1/n}\left(\frac{n}{n+1}\right)\left[\left(\frac{h}{2}\right)^{\frac{1+n}{n}} - y^{\frac{1+n}{n}}\right] \quad (3)$$

Integrating the velocity profiles from equation (2) and (3) over the corresponding cross-sectional flow areas results in the volumetric flow rates $\dot{V}_P$ for the pipe flow (Equation (4)) and $\dot{V}_G$ for the gap flow (Equation (5)), respectively. The cross-sectional flow area of the inner channel is circular with constant radius R.

$$\dot{V}_P = \int_0^R 2\pi r u_P(r)dr = \left(\frac{\pi n}{3n+1}\right)\left(\frac{1}{2K}\left|\frac{dp}{dx}\right|\right)^{1/n}\left(R^{\frac{1}{n+3}}\right) \quad (4)$$

The cross-sectional flow area of the adhesive fill gap is the lateral surface area of a cylinder with the thickness h and the radius w. The radius w is the adhesive propagation radius in the fill gap, as it describes the radial expansion of the adhesive upon exit from an inner channel.

$$\dot{V}_G = 2\int_0^{\frac{h}{2}} 2\pi w u_G(y)dy = \frac{\left(2\pi n w h^{\frac{2n+1}{n}}\right)\left(\frac{1}{4K}\left|\frac{dp}{d\vartheta}\right|\right)^{1/n}}{(2n+1)} \quad (5)$$

The maximum pressure of the injection device p_{ID} is equal to the sum of the pressure loss due to the adhesive pipe flow through an inner channel with length l and the pressure loss due to the adhesive gap flow in the fill gap along the radius of propagation w (Equation (6)).

$$p_{ID} = \Delta p_P + \Delta p_G = \left|\frac{dp}{dx}\right| * l + \left|\frac{dp}{d\vartheta}\right| * w \quad (6)$$

The system of equations (4), (5) and (6) is solved numerically for $w = w_{min}$ using $R = R_i$ and $l = l_{max}$, where R_i is the minimum manufacturable inner channel radius. It is recommended to use R_i for the inner channel radius to minimize the reduction of both the load bearing capacity of the PBF-LB/M part and the connecting surface area A_{con} of the PBF-LB/M part. The maximum distance l_{max} between the adhesive inlet and the furthest adhesive outlet is the sum of the shortest distance from the adhesive inlet to the fill gap and half of the connecting surface perimeter. Solving for w using $R = R_i$ and $l = l_{max}$ yields the minimum radius of propagation w_{min} as a function of a constant adhesive fill gap thickness h.

2.3. Phase 3: Inner channel layout in the PBF-LB/M part

A preliminary inner channel layout is designed by covering the connecting surface of the PBF-LB/M part having the surface area A_{con} with a equidistant circles having the radius w_{min}. The center of each circle corresponds to the position of an adhesive outlet to the adhesive fill gap. The minimum number of circles a should be determined using equation (7).

$$a > \frac{A_{Con}}{{w_{min}}^2\pi} \qquad a \in \mathbb{N}_e = \{2,4,6,\dots,\infty\} \quad (7)$$

The restriction of a to even numbers leads to the ideal symmetrical arrangement of the outlets across the connecting surface.

Inner channels with radius R_i and a 45°-droplet-like cross section are subsequently designed within the PBF-LB/M part to connect each adhesive outlet with the adhesive inlet, ensuring that the maximum channel length does not exceed l_{max} and the total length of all inner channels is kept to a minimum. Additionally, it must be ensured that the PBF-LB/M part complies with a material- and machine-dependent minimum wall thickness of 0.3 to 1.0 mm [3].

2.4. Phase 4: Validation of the inner channel layout

The last phase validates the preliminary inner channel layout in terms of pressure loss and complete coverage of the adhesive fill gap with adhesive. Suitable methods can be both the generation of physical visualization models and virtual simulation models. Physical models of the adherents made from transparent synthetic resin by means of stereolithography can be used to visualize the adhesive flow in the inner channels and the fill gap. This type of validation can be implemented with minimal effort, but quantification of the results is hardly possible. Using the CAD model of the inner channels infill and the adjacent adhesive fill gap geometry in volumetric form enables a multiphase CFD analysis. The modeling effort is more complex than using physical models, but the adhesive

propagation in the fill gap can be quantified, which makes it easier to derive design improvements.

3. Implementation and results

Following the method described in section 2, the adhesive application by injection into additively manufactured inner channels is demonstrated on a circular adhesive SLJ between a PBF-LB/M sleeve made of aluminum alloy AlSi10Mg (outside adherent) and a circular CFRP tube (inside adherent). The adhesive inlet is located on the exterior of the PBF-LB/M part and a 2-component construction adhesive based on epoxy resin (*3M Scotch-Weld DP490*) was chosen as the adhesive. The injection into the PBF-LB/M sleeve is carried out using a manually operated adhesive injection device with an attached mixing nozzle. Figure 2 shows a schematic of all the components and dimensions of the SLJ.

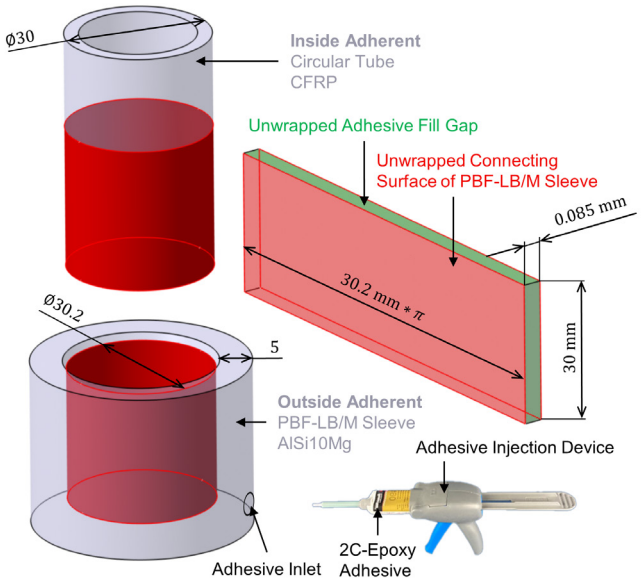

Figure 2: Circular adhesive SLJ considered for demonstrating the adhesive application by injection into inner channels

According to the adhesive manufacturer's specifications [16] and consistent with [17], the adhesive fill gap thickness was set to $h = 0.1$ mm. As the adherents' inner and outer diameter are subjected to manufacturing tolerances, the actual minimum inner diameter of the PBF-LB/M sleeve was measured optically using a 3D-scanner (*Keyence VL-500*) as $d_{min} = 30.170$ mm. The maximum outer diameter of the aluminum round bar was taken from the manufacturer's tolerance specifications of Ø30h9 as $D_{max} = 30.000$ mm. Therefore, the minimum gap thickness is $h = 0.085$ mm.

Phase 1. The maximum pressure of the injection device was measured with a digital pressure gauge (*otom DIGI-10*) with a measuring range of 0 to 100 bar. The pressure gauge was connected to the injection device via hydraulic fittings. The volume inside the fittings was filled with HLP ISO-VG 46 mineral oil before connecting the injection device to prevent contamination of the gauge with adhesive. The maximum pressure that can be exerted with the injection device was determined to $p_{ID} = 18.9$ bar.

The maximum volumetric flow rate of the injection device was determined by injecting the adhesive with maximum pressure onto an electronic precision scale (*Sartorius U 4600*) for 20 consecutive times over a duration of 3 s. The average mass flux was measured as $\dot{m}_{ID} = 0.37$ g/s. Dividing the mass flux by the adhesive´s density of $\rho_{DP490} = 1.0$ g/cm^3 [16] yields a volumetric flow rate of $\dot{V}_{ID} = 0.37 \times 10^{-6}$ m^3/s.

The shear rate $\dot{\gamma}$ - shear stress τ dependency of the adhesive was determined through rheological measurements according to [18]. A rotational rheometer (*TA Instruments HR 30*) was used for measuring the torque required for shearing the adhesive between two concentric cylinders (one stationary, one pivotable) at different rotational speeds [19]. From the rotational speed, torque, cylinder radius and cylinder distance, the associated nominal shear rates $\dot{\gamma}$ and nominal shear stresses τ in the adhesive were derived. From this data, the flow consistency index $K = 185.1$ Pa · s and the flow behavior index $n = 0.31$ were determined by regression analysis.

Phase 2. By adding the outside adherent´s wall thickness of $t_{OA} = 5$ mm to half of the connecting surface perimeter of $p_{CS} = (30.2 * \pi + 30)$ mm the maximum distance between the adhesive inlet and the adhesive fill gap results to $l_{max} = 130$ mm. Along with the minimum manufacturable inner channel radius $R_i = 1.0$ mm [10], the minimum radius of propagation was calculated by numerically solving the system of equations (4), (5) and (6) as $w_{min} = 10.9$ mm using the function *vpasolve* implemented in the numeric computing environment *MATLAB (MathWorks)*.

Phase 3. The two-step process of generating a preliminary channel layout in the outer adherent is depicted in Figure 3. The unwrapped connecting surface of the PBF-LB/M sleeve was covered with $a = 8$ (Equation (7)) equally spaced circles with radius w_{min}. Inner channels with a radius of $R_i = 1.0$ mm and a 45°-droplet-like cross section were then designed in the PBF-LB/M sleeve to connect the center of each circle to the adhesive inlet with a layout that does not remove more material than necessary. Four outlets located in the same plane (perpendicular to the longitudinal axis of the circular SLJ) were attached to two semi-circular inner channels located midway between the connecting surface and the exterior surface of the PBF-LB/M sleeve. The semi-circular inner channels of each level are interconnected with a level connector channel, which is attached midway between the four outlets of each level, respectively.

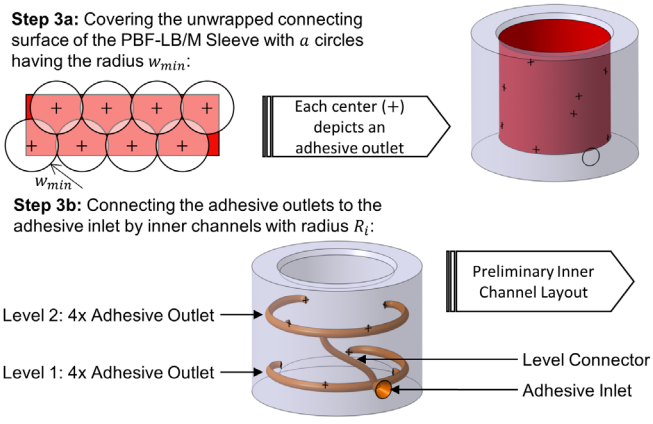

Figure 3: The two-step process of generating the geometry model of a preliminary inner channel layout

Phase 4. With the geometry model of the preliminary channel layout obtained from Phase 3, a pseudo-transient, implicit CFD analysis according to the volume of fluid (VOF) method [20] was carried out using the software Ansys Fluent. The injection device is modeled with an inlet extension with a length of ten times the inlet diameter (CFD inlet). The adhesive flows from the injection device, through the inner channels into the fill gap, and may exit the flow domain through the top lateral surface of the fill gap (CFD outlet) (Figure 4). Discretization was done with polyhedral elements with a minimum of seven elements for the adhesive fill gap thickness. The material properties of the adhesive are modeled using the Ostwald-de Waele power law using the parameters obtained from Phase 1. The simulation starts with the flow domain filled with the primary phase (air). Subsequently, the secondary phase (adhesive) flows with a constant mass flux of $\dot{m}_{in} = \dot{m}_{ID}$ through the inlet extension into the inner channels and the adhesive fill gap. A relative pressure of $p_{out} = 0$ bar is set as a boundary condition (BC) at the CFD outlet. The simulation converges when the adhesive flows out of the CFD outlet with the mass flux specified at the inlet.

It is confirmed that the total pressure loss due to the adhesive flow does not exceed the maximum pressure of the injection device, as the CFD-calculated pressure in a state of convergence at the adhesive inlet $p_{in} = 9.1$ bar (Figure 4) is lower than the maximum pressure of the injection device p_{ID} ($p_{in} < p_{ID}$) indicating that Phase 3 was carried out correctly.

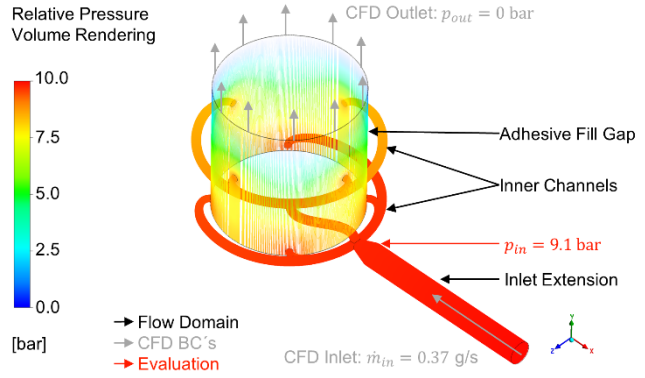

Figure 4: Volume Rendering of the relative pressure with respect to the depicted CFD boundary conditions

In the VOF method, an additional equation for the filled fraction of each control volume is solved [21] to determine the volume fraction (VF) of each phase of the multiphase model for each element of the flow domain. Evaluation of the adhesive´s VF through the contour plot in Figure 5 (top left) shows air inclusions. This is attributable to the simultaneous circular propagation of the adhesive fronts originating from outlets of the 1st and 2nd level, trapping 6.6% of the total fill gap air volume.

The results from the CFD analysis were used to improve the preliminary inner channel layout with an additional outlet on each level to diminish the circular shape of the adhesive fronts and a longer level connector to attach the 2nd level opposite the adhesive inlet to delay the adhesive exit from the 2nd level outlets. The results of a CFD analysis with the improved channel layout show that the total fill gap air was reduced to 3.9% (Figure 5, top right). Moreover, the number of computational iterations to reduce the fill gap air to 6.6% is halved compared to the preliminary channel layout (Figure 5, bottom).

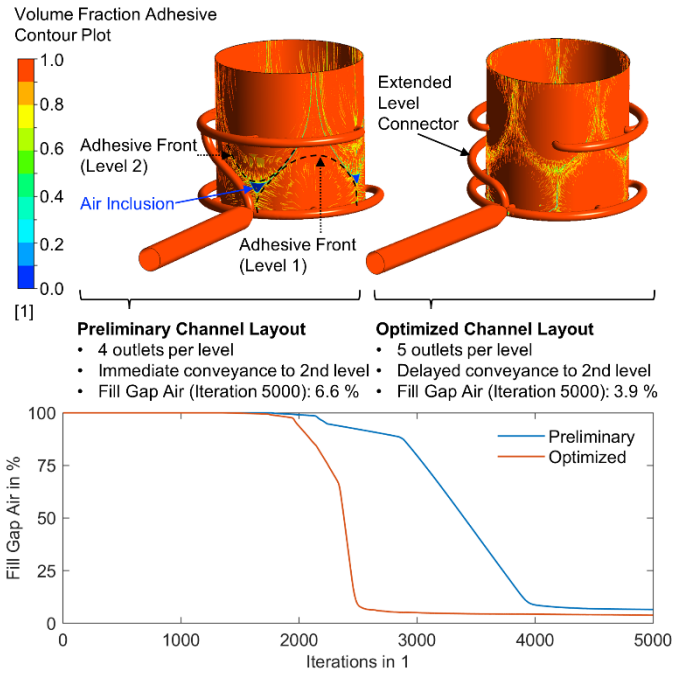

Figure 5: Contour plot of the adhesive´s volume fraction in a state of convergence for differing channel layouts (top) and total fill gap air as a function of computational iterations (bottom)

To further decrease the total fill gap air in a state of convergence, additional design improvements like varying the distance between the 1st and the 2nd level or placing additional venting holes in the PBF-LB/M sleeve to release trapped air from the fill gap can be implemented and validated through further CFD analysis. The necessity for additional design optimization iterations depends on the requirements placed on the joint (e.g., bond strength, impermeability), as well as the available resources, and must be assessed for each specific application.

4. Conclusion

With the overall objective of facilitating adhesive application in adhesively bonded joints involving PBF-LB/M parts, a method for the design of inner channels intended for adhesive application by injection was presented and successfully applied to an example joint. Provided that the connecting surface of the PBF-LB/M part, a constant adhesive fill gap thickness, an accessible adhesive inlet in the PBF-LB/M part, and the intended adhesive and adhesive injection device can be identified beforehand, the four-step method leads to a CAD model of the PBF-LB/M part containing inner channels which can be used to apply the adhesive to the adhesive fill gap between the pre-aligned adherents by injection into a single adhesive inlet. The method includes the sequential characterization of the adhesive and the injection device (Phase 1), calculation of the adhesive´s minimum radius of propagation in the fill gap upon exit from an inner channel

(Phase 2), creation of a preliminary inner channel layout (Phase 3), and validation of the layout in terms of complete coverage of the adhesive fill gap with adhesive (Phase 4). As part of an optimization iteration, design improvements resulting from Phase 4 can be used as feedback to Phase 3 to further improve the inner channel layout. The preliminary channel layout of the example joint was validated by CFD analysis with the first design optimization iteration, leading to a reduction of the residual air volume in the adhesive fill gap by 41%. Application of this method, therefore, ensures optimal adhesive coverage, which opens the possibility of manufacturing larger and more complex PBF-LB/M parts or supplementing PBF-LB/M parts with other parts (e.g., CFRP parts) to form high-quality structures. Future work could aim to apply the method proposed to other AM technologies, materials [22] and joint geometries (e.g., butt joints or double lap joints) considering the respective manufacturing constraints. Furthermore, the effect of the method proposed on the bonding strength can be quantified by comparing test joints which were joined using different adhesive application methods (e.g., pre-application) in the course of static tensile tests.

Acknowledgements

This research is part of the project FLAB-3Dprint and funded by dtec.bw – Digitalization and Technology Research Center of the Bundeswehr which we gratefully acknowledge. dtec.bw is funded by the European Union – NextGenerationEU.

References

[1] DIN EN ISO/ASTM 52911-1:2020-05. Additive manufacturing – Design – Part 1: Laser-based powder bed fusion of metals. Berlin: Beuth; 2020.
[2] Li C, Liu ZY, Fang XY. Residual Stress in Metal Additive Manufacturing. Procedia CIRP 2018;71:348–353. https://doi.org/10.1016/j.procir.2018.05.039.
[3] Diegel O, Nordin A, Motte D. A Practical Guide to Design for Additive Manufacturing. Singapore: Springer; 2018.
[4] Yang L, Hsu K, Baughman B. Additive Manufacturing of Metals: The Technology, Materials, Design and Production. Cham: Springer International Publishing; 2017.
[5] Reichwein J, Kirchner E. Part orientation and separation to reduce Process Costs in Additive Manufacturing. Proc Des Soc 2021;1:2399–2408. https://doi.org/10.1017/pds.2021.501.
[6] DVS 3320. Quality requirements in adhesive application. Duesseldorf: DVS Media; 2012.
[7] Pietropaoli M, Ahlfeld R, Montomoli F. Design for Additive Manufacturing: Internal Channel Optimization. J Eng Gas Turbines Power 2017;139. https://doi.org/10.1115/1.4036358.
[8] DVS 1401. Gestaltungsempfehlungen zum Kleben additiv gefertigter Bauteile. Duesseldorf: DVS Media; 2021.
[9] Baier M, Sinico M, Witvrouw A. A novel tomographic characterisation approach for sag and dross defects in metal additively manufactured channels. Addit Manuf 2021;39:101892. https://doi.org/10.1016/j.addma.2021.101892.
[10] Kolb T, Mahr A, Huber F. Qualification of channels produced by laser powder bed fusion: Analysis of cleaning methods, flow rate and melt pool monitoring data. Addit Manuf 2019;25:430–436. https://doi.org/10.1016/j.addma.2018.11.026.
[11] Adam G, Zimmer D. Design for Additive Manufacturing—Element transitions and aggregated structures. CIRP J Manuf Sci Technol 2014;7:20–28. https://doi.org/10.1016/j.cirpj.2013.10.001.
[12] Mazur M, Leary M, McMillan M. SLM additive manufacture of H13 tool steel with conformal cooling and structural lattices. RPJ 2016;22:504–518. https://doi.org/10.1108/RPJ-06-2014-0075.
[13] Ascher M, Späth R (2021) Joining Technology of Additively Manufactured Components: Design Measures for Optimizing the Strength of Adhesively Bonded Joints. In: Lachmayer R, Behrend B, Kaierle S, editors. Innovative Product Development by Additive Manufacturing. Berlin: Springer; 2022. https://doi.org/10.1007/978-3-031-05918-6_5.
[14] Cloete M. Modelling of non-Newtonian fluid flow through and over porous media with the inclusion of boundary effects. Stellenbosch: Stellenbosch University; 2013.
[15] Harrell JFE. Regression Modelling Strategies: With Applications to Linear Models, Logistic and Ordinal Regression and Survival Analysis. Cham: Springer; 2015.
[16] Material Data Sheet: Scotch-Weld DP 490. Neuss: 3M Deutschland GmbH; 2003.
[17] Habenicht G. Applied adhesive bonding: A practical guide for flawless results. Weinheim: Wiley-VCH; 2009.
[18] DIN EN 12092:2002-02. Adhesives – Determination of viscosity. Berlin: Beuth; 2002.
[19] DIN EN ISO 3219-2:2021-08. Rheology – Part 2: General principles of rotational and oscillatory rheometry. Berlin: Beuth; 2021.
[20] Hirt C, Nichols B. (1981) Volume of fluid (VOF) method for the dynamics of free boundaries. J Comp Phys 1981;39:201–225. https://doi.org/10.1016/0021-9991(81)90145-5.
[21] Ferziger JH, Perić M, Street RL. Computational Methods for Fluid Dynamics. Cham: Springer International Publishing; 2020.
[22] Bourell D, Kruth JP, Leu M. Materials for additive manufacturing. CIRP Annals 2017;66:659–681. https://doi.org/10.1016/j.cirp.2017.05.009.